

# High-Isolated Full-Duplex Dongle Antenna Based on Even-Mode Suppression for B5G Communications

Yiran Da<sup>1</sup>, Xiaoming Chen<sup>1</sup>, Aofang Zhang<sup>2</sup>, Kunpeng Wei<sup>2</sup>, and Ahmed A. Kishk<sup>3</sup>

<sup>1</sup>School of Information and Communications Engineering  
Xi'an Jiaotong University, Xi'an, 710049, China  
dyr916@stu.xjtu.edu.cn, xiaoming.chen@mail.xjtu.edu.cn

<sup>2</sup>Honor Device Co. Ltd, Beijing, 100095, China  
aofangzhang@foxmail.com, weikunpeng\_2013@tsinghua.org.cn

<sup>3</sup>Concordia University, Montreal, QC H3G 1M8, Canada  
kishk@encs.concordia.ca

**Abstract** – A space-shared full-duplex antenna with high isolation is proposed for universal serial bus (USB) dongles. A compact antenna with a compact size of 22 mm × 4 mm comprises a loop and dipole antennas, working as a vertical monopole and a horizontal dipole, respectively. The dipole-type is fed by a microstrip-slotline transition with filtering characteristics of odd-mode bandpass and even-mode bandstop, avoiding the even-mode excitation for the loop antenna. The inherent isolation is caused by the orthogonality of the modes and the even-mode suppression (caused by the microstrip-slotline transition). Thus, high port isolation, low envelope correlation coefficients (ECC), and high efficiency are achieved across the 5G band of 3.4-3.6 GHz.

**Index Terms** – even-mode suppression, full-duplex dongle antenna, high isolation.

## I. INTRODUCTION

With the growing demands for mobile communication, the fifth-generation (5G) communication technology has become famous for its high capacity and low latency [1]. The 5G antennas have been extensively studied [2]. A universal serial bus (USB) dongle is an Internet access module with a USB interface that can provide a network connection for laptops. Full-duplex antennas could effectively multiply the spectrum efficiency by transmitting and receiving signals within the same frequency band and time slot [3, 4], making them a key enabler for beyond 5G (B5G) technology. Therefore, compact full-duplex antennas are highly desirable for USB dongles. For reliable full-duplex communications, a 100-dB isolation between the transmitter and receiver is typically

required. Such high isolation is usually achieved by a combination of antenna isolation enhancement, analog filtering, and digital interference cancellation [5]. Therefore, antennas with high isolations (> 25 dB) are desired to relieve the pressure on the sequential processing and improve the dynamic range of the wireless connectivity [6, 7].

Various isolation improvement methods have been proposed for closely arranged antennas [8–26]. The first type is the decoupling method based on partition, such as electromagnetic bandgap structure [8, 9], decoupling resonators [10, 11], and defected ground structures [12, 13]. The second type is the decoupling method based on neutralization, such as array decoupling surface [14], decoupling ground [15–17], dielectric superstrate [18, 19], and decoupling networks [20, 21]. The partition and neutralization based decoupling methods are combined in [22] to enhance the decoupling bandwidth. In these papers, the antenna elements are separated, and the additional decoupling structures occupy extra specified space, making them less suitable for USB dongles. In [23], good isolation is obtained by sharing one common grounding branch for two adjacent antennas. The orthogonal modes of the antenna pair are utilized to improve the isolation in [24, 25]. Although the self-decoupling is achieved within a compact space, spatial reuse is still not well addressed, and, more importantly, the resulting isolations are insufficient for full-duplex communications. The mode cancellation method has been proposed to decouple the patch antenna pair with the shared radiator [26]. However, the operating frequency band is narrow. It is necessary to enhance the port isolation further to meet the higher requirement of full-duplex communication. Performance comparisons of different terminal antennas are shown in Table 1.

Table 1: Performance comparison

Ref.	Freq. (GHz)	Ant. Size (mm <sup>2</sup> )	Isolation	Effi.	ECC
[23]	3.4-3.6	20×7	17 db	58%	0.1
[25]	3.4-3.6	12×7	20 db	51%/74%	0.06
[26]	4.8-4.9	15.4×15.5	25 db	80%	0.02
This work	3.4-3.6	22×4	30 db	79%/64%	0.003

For fairness, the size and isolation of the compact arranged antenna pair are compared instead of MIMO antennas.

The microstrip-slotline transition structures are usually employed for filtering antennas, whose inherent characteristic of common-mode suppression can simplify the design procedure of the filtering antennas (only differential-mode passband performance needs to be studied) [27, 28]. In this paper, and different from previous papers, the microstrip-slotline transition structure is utilized to improve the isolation of the full-duplex antenna pair.

Here, a high-isolated full-duplex antenna for USB dongles is proposed, which consists of a tightly arranged loop antenna (vertical monopole mode) and dipole antenna (horizontal dipole mode). The dipole is fed by a  $\Gamma$ -shaped microstrip-slotline transition, avoiding the even-mode excitation of the loop antenna and maintaining the odd-mode feeding for the dipole. High port isolation is obtained owing to the mode orthogonality of the elements and the even-mode suppression of the microstrip-slotline transition. Within the operating frequency band of 3.4-3.6 GHz, high isolation (> 30 db) and low envelope correlation coefficient (ECC) (< 0.003) are achieved, exhibiting superior performances.

## II. HIGH-ISOLATED FULL-DUPLEX DONGLE ANTENNA WITH MICROSTRIP-SLOTLINE TRANSITION

### A. Array configuration

The configuration of the proposed full-duplex antenna is shown in Fig. 1 (a), which is composed of a loop antenna (Antenna 1) and a dipole antenna (Antenna 2). The loop antenna and the  $\Gamma$ -shaped microstrip feeding line are printed on the top side of the F4B substrate (with a relative permittivity of 4.4, a loss tangent of 0.002, and a thickness of 1 mm), while the dipole-type antenna and the ground plane are printed on the bottom side of the F4B substrate. The arms of the dipole are bent to reduce the antenna size. The two independent elements are tightly arranged in a single board of 22 mm × 4 mm,

simultaneously serving as the receiving and transmitting antennas. As shown in Fig. 1 (b), one end of the loop antenna is shorted to the ground plane, and a coaxial cable directly feeds the other end (Port 1). A  $\Gamma$ -shaped microstrip-slotline transition feeds the dipole antenna. The slotline on the ground plane of the FR4 substrate intersects orthogonally with the  $\Gamma$ -shaped microstrip line on the opposite interface, forming a transition from the microstrip feeding line to the slotline.

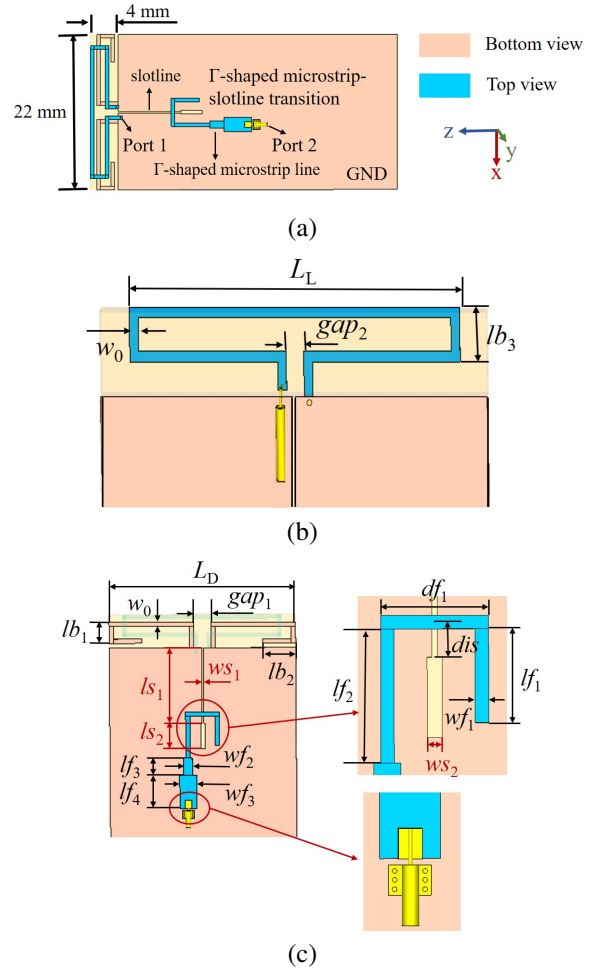


Fig. 1. Configurations of (a) Proposed full-duplex dongle antenna, (b) Loop antenna (Antenna 1), and (c) Dipole (Antenna 2). Optimized parameters are:  $L_D = 22$ ,  $L_L = 18.8$ ,  $w_0 = 0.5$ ,  $gap_1 = 2$ ,  $gap_2 = 1$ ,  $lb_1 = 2.5$ ,  $lb_2 = 3.9$ ,  $lb_3 = 2.6$ ,  $ls_1 = 9$ ,  $ls_2 = 3$ ,  $ws_1 = 0.2$ ,  $ws_2 = 0.55$ ,  $lf_1 = 3.5$ ,  $lf_2 = 5$ ,  $lf_3 = 2$ ,  $lf_4 = 4$ ,  $df_1 = 4$ ,  $wf_1 = 0.5$ ,  $wf_2 = 1$ ,  $wf_3 = 2$ ,  $dis = 1$  (all dimensions in mm).

The current distributions of Antennas 1 and 2 at the center frequency (3.5 GHz) are shown in Figs. 2 (a) and (b), respectively. On the dipole, the currents along the dipole arms parallel to the ground plane edge are in the same direction and at the feeding region are opposite

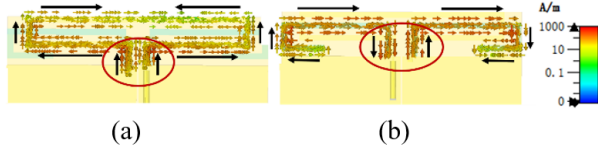


Fig. 2. Surface current distributions at 3.5 GHz. (a) Loop antenna excited by Port 1 (monopole mode). (b) Dipole antenna excited by Port 2 (dipole mode).

to each other (circled), exhibiting odd-mode excitation, while the currents flowing on the loop edges parallel to the ground plane edge are opposite to each other and at the feeding region are on the same direction exhibiting an even-mode excitation. Thus, the loop antenna operates as a vertical monopole. Therefore, the dipole antenna works as a horizontal dipole. Due to the orthogonal current mode of Antenna 1 (vertical monopole mode) and Antenna 2 (horizontal dipole mode), the mutual coupling between the two elements is reduced, thus, improving the port isolation of the full-duplex antenna. To further enhance the port isolation, the  $\Gamma$ -shaped microstrip-slotline transition is utilized to feed the dipole antenna, avoiding the even-mode excitation for the loop antenna and maintaining the odd-mode feeding for the dipole antenna.

**B. Microstrip-slotline transition**

Figure 3 illustrates the electric field distributions of the microstrip-slotline transition. Under the odd-mode excitation, two ends of the microstrip line are excited with equal amplitude and opposite phases. Thus, the electric fields distributed on both sides of the slotline are opposite, as shown in Fig. 3 (a). A virtual electric wall is produced at the center of the slotline, and a vertical electric field is generated through strong magnetic coupling. Therefore, the odd-mode signal flowing along the microstrip can be transformed into the slotline mode (vertical electric field) and transmitted to the antenna along the slot. Under the even-mode excitation, the two ends of the microstrip line are excited with equal amplitude and phase. Therefore, the directions of the electric fields on both sides of the slotline are the same,

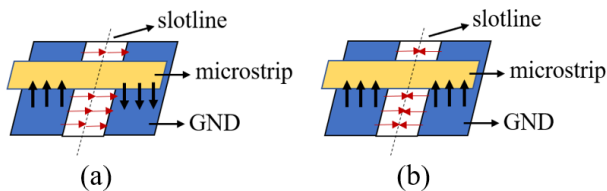


Fig. 3. Electric field distributions of the microstrip-slotline transition with (a) odd-mode excitation and (b) even-mode excitation.

as shown in Fig. 3 (b). A virtual magnetic wall is produced at the center of the slotline, and the vertical electric fields generated by the even-mode signals are canceled by each other on the slotline. Thus, there is nearly no vertical electric field passing through the slot, indicating that the even-mode signals are difficult to pass through the microstrip-slotline transition. It is concluded that the microstrip-slotline transition has good properties of odd-mode transmission and even-mode suppression.

To investigate the mechanism of the odd-mode transmission, the arms of the bent dipole are excited by odd-mode signals (Port-1), and Port-2 feeds the  $\Gamma$ -shaped microstrip-slotline transition, as shown in Fig. 4 (a). Figure 4 (b) shows the simulated reflection coefficients ( $S_{11}$ ), and coupling ( $S_{21}$ ) of the antenna as the length of the slotline ( $l_{s1}$ ) varies. When the length of the slotline is around a quarter wavelength, the odd-mode transmission coefficient of  $S_{12}$  will reach its maximum. Thus, the odd-mode transmission is optimal at this point. To investigate the principle of even-mode suppression, the ends of the loop antenna are excited by even-mode signals (Port-1), and the  $\Gamma$ -shaped microstrip-slotline transition is fed through Port-2, as illustrated in Fig. 5 (a). Figure 5 (b) shows the simulated reflection coefficients ( $S_{11}$ ) and coupling ( $S_{21}$ ) of the antenna with varying  $l_{s1}$ . When the slotline’s length is about a quarter wavelength, the curve of even-mode transmission coefficient  $S_{12}$  will produce a notch. Thus, the optimal even-mode suppression is achieved at this point. Moreover, the microstrip-slotline transition affects the reflection

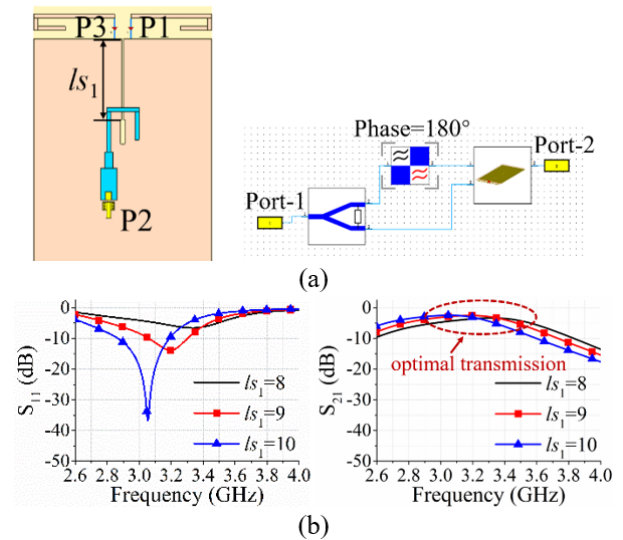


Fig. 4. Investigation of odd-mode transmission. (a) Odd-mode excitation for the dipole antenna. (b) Simulated reflection coefficients ( $S_{11}$ ) and coupling ( $S_{21}$ ) with varied  $l_{s1}$ . (Unit: mm).

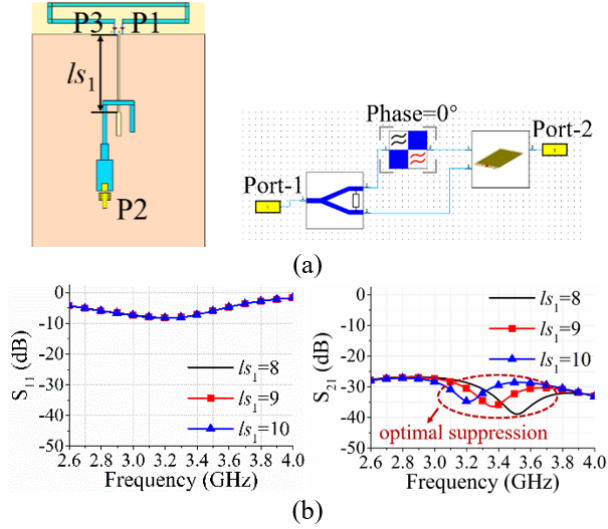


Fig. 5. Investigation of even-mode suppression. (a) Even-mode excitation for the loop antenna. (b) Simulated reflection coefficients ( $S_{11}$ ) and coupling ( $S_{21}$ ) with varied  $l_{s1}$ . (Unit: mm).

coefficient of the odd-mode excited antenna while not affecting the matching performance of the even-mode excited antenna.

Therefore, when the tightly arranged elements of the full-duplex antenna are excited by even-mode and odd-mode signals, respectively, the microstrip-slotline transition can be employed to achieve optimal odd-mode transmission and even-mode suppression. This results in a bandpass filtering characteristic for odd-mode excitation and a bandstop filtering characteristic for even-mode excitation, further improving the port isolation, which is different from the traditional decoupling methods based on mode cancellation method (MCM) [26, 29, 30].

### III. DESIGN PROCEDURE AND RESULTS DISCUSSION

#### A. Design procedure

To obtain high isolation and good impedance matching, the design parameters of the  $\Gamma$ -shaped microstrip-slotline transition of the proposed full-duplex antenna are studied. The stepped slotline helps to miniaturize the size, and the stepped microstrip feeding line contributes to impedance matching. Figure 6 shows the simulated reflection coefficient ( $S_{22}$ ) of the dipole and coupling ( $S_{21}$ ) of the antenna with varied  $l_{s1}$  and  $w_{s1}$ . Since the matching performance of the loop-type antenna is not affected by the  $\Gamma$ -shaped microstrip-slotline transition, the simulated reflection coefficients ( $S_{11}$ ) of the loop antenna are omitted here for clarity. As observed, the resonant frequency of the dipole-

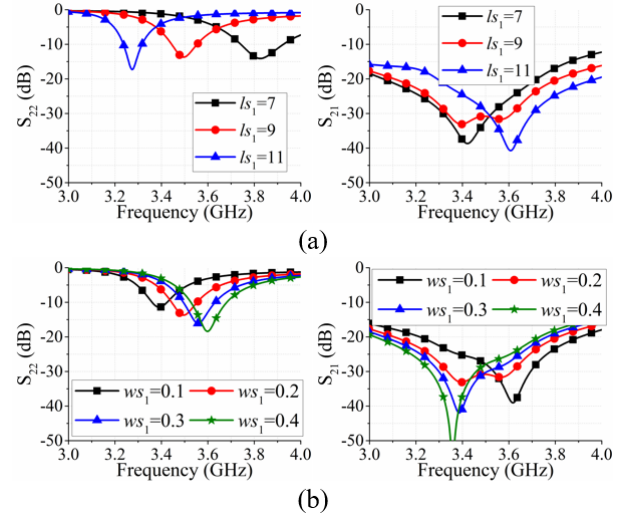


Fig. 6. Simulated reflection coefficient ( $S_{22}$ ) and coupling ( $S_{21}$ ) of the antenna with (a) varied  $l_{s1}$  and (b) varied  $w_{s1}$ . (Units: mm).

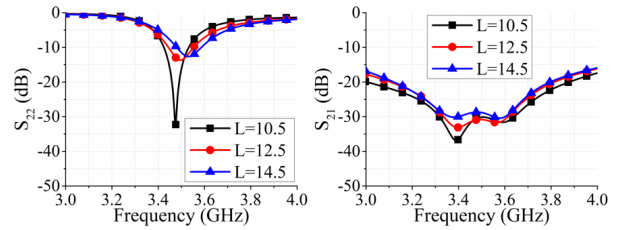


Fig. 7. Simulated reflection coefficient ( $S_{22}$ ) and coupling ( $S_{21}$ ) of the antenna with varied  $L$ . (Unit: mm).

type antenna decreases by increasing  $l_{s1}$  and decreasing  $w_{s1}$ , and the port isolation also changes accordingly. When the slotline's length is about a quarter wavelength, good impedance matching, and high isolation can be achieved. The impedance of the microstrip line is mainly determined by its width, and the length of the  $\Gamma$ -shaped microstrip line ( $L = lf_1 + df_1 + lf_2$ ) is studied in Fig. 7. It can be seen that the length of the  $\Gamma$ -shaped microstrip line mainly affects the impedance bandwidth, but has little effect on the resonant frequency of the dipole and the port isolation of the antenna. According to the parametric studies,  $L = 12.5$  mm (about a quarter wavelength) is selected to obtain a wider impedance bandwidth.

In conclusion, the matching performance (such as the resonant frequency and the impedance bandwidth) of the dipole antenna mainly depends on the sizes of the slotline and the microstrip line. The port isolation is determined by the even-mode suppression of the  $\Gamma$ -shaped microstrip-slotline transition, which mainly depends on the length and width of the slotline.

The optimized dimensions of the proposed full-duplex antenna are listed in the caption of Fig. 1.

**B. Results discussion**

Figure 8 shows the top and bottom views of the fabricated antenna. Two 50Ω coaxial cables are used to feed the two ports of the full-duplex antenna. The simulated and measured S-parameters of the antenna are shown in Fig. 9 (a). It can be seen that, across the desired frequency band of 3.4 to 3.6 GHz, the reflection coefficients

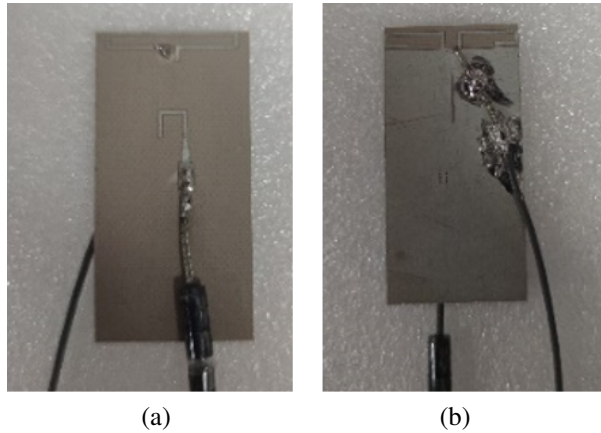


Fig. 8. Photographs of the prototype. (a) Top view. (b) Bottom view.

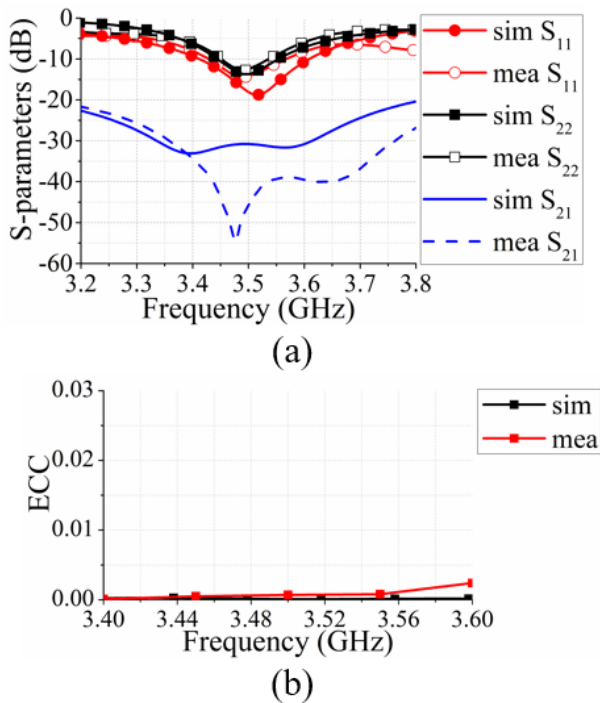


Fig. 9. Simulated and measured (a) S-parameters and (b) ECC of the antenna.

( $S_{11}$  and  $S_{22}$ ) of the loop (Antenna 1) and the dipole (Antenna 2) are maintained below -6 db, and the port isolation of the antenna is above 30 db over the entire good agreement. Figure 9 (b) illustrates the simulated and bandwidth. The simulation and measurement results are in measured envelope correlation coefficients (ECCs) from the simulated and measured radiation patterns [31]. The ECCs are less than 0.003 within the operating band, showing an excellent diversity performance. The normalized simulated and measured radiation patterns of Antenna 1 and Antenna 2 at the frequency of 3.5 GHz are shown in Fig. 10. The measured radiation patterns are consistent with the simulation results. In addition, the simulated and measured efficiencies at different frequencies are listed in Table 2. The simulation and measurement results are about the same, and the small discrepancies between them are mainly caused by manufacturing tolerance, imperfect soldering, and measurement errors. As observed, good efficiencies of 79% ~ 91% are achieved when fed through Port 1, and decent efficiencies of 64% ~ 83% are achieved when fed through Port 2, indicating satisfactory radiation performances of the proposed antenna.

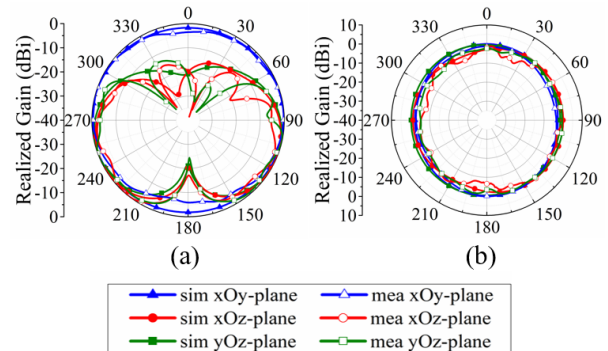


Fig. 10. Simulated and measured radiation patterns at 3.5 GHz of (a) Antenna 1 and (b) Antenna 2.

Table 2: Measured and simulated efficiencies of the antenna at different frequencies

Freq. (GHz)	3.40	3.45	3.50	3.55	3.60
Sim. Effi. (P1)	85%	92%	95%	91%	88%
Mea. Effi. (P1)	80%	87%	91%	85%	79%
Sim. Effi. (P2)	70%	82%	87%	84%	75%
Mea. Effi. (P2)	64%	80%	83%	81%	69%

#### IV. CONCLUSION

This article presents a full-duplex dongle antenna composed of a tightly arranged loop antenna and dipole antenna. High port isolation has been obtained thanks to the orthogonal modes of the elements and the even-mode suppression of the microstrip-slotline transition. The working mechanism and the design procedure of the  $\Gamma$ -shaped microstrip-slotline transition were well studied. The proposed antenna has been manufactured for experimental verification. The simulation and measurement results were in reasonable agreement. High isolation ( $>30$  db), low ECC ( $<0.003$ ), and high efficiency ( $>79\%/64\%$ ) were observed over the desired 5G frequency band from 3.4 to 3.6 GHz. Therefore, the proposed full-duplex dongle antenna with high isolation and compact size is suitable for B5G communications.

#### REFERENCES

- [1] A. Zaidi, F. Athley, J. Medbo, U. Gustavsson, and G. Durisi, *5G Physical Layer: Principles, Models and Technology Components*, Academic Press, London, U.K., 2018.
- [2] R. Hussain and M. S. Sharawi, "5G MIMO antenna designs for base station and user equipment: some recent developments and trends," *IEEE Antennas Propag. Mag.*, vol. 64, no. 3, pp. 95-107, Jun. 2022.
- [3] A. Sabharwal, P. Schniter, D. Guo, D. W. Bliss, S. Rangarajan, and R. Wichman, "In-band full-duplex wireless: Challenges and opportunities," *IEEE J. Sel. Areas Commun.*, vol. 32, no. 9, pp. 1637-1652, Sep. 2014.
- [4] D. Kim, H. Lee, and D. Hong, "A survey of in-band full-duplex transmission: From the perspective of PHY and MAC layers," *IEEE Commun. Surveys Tuts.*, vol. 17, no. 4, pp. 2017-2046, 4th Quart., 2015.
- [5] S. B. Venkatakrisnan, A. Hovsepian, A. D. Johnson, T. Nakatani, E. A. Alwan, and J. L. Volakis, "Techniques for achieving high isolation in RF domain for simultaneous transmit and receive," *IEEE Open J. Antennas Propag.*, vol. 1, pp. 358-367, Jul. 2020.
- [6] J. H. Zhang, F. M. He, W. Li, and Y. Li, "Self-interference cancellation: A comprehensive review from circuits and fields perspectives," *Electron.*, vol. 11, no. 2, pp. 172, Jan. 2022.
- [7] F. Peng, F. Peng, F. Yang, B. Liu, and X. Chen, "Experimental investigation of decoupling effect on the nonlinearity of power amplifiers in transmitter array," *Applied Computational Electromagnetics Society (ACES) Journal*, in press.
- [8] L. Zhao, Y. He, G. Zhao, X. Chen, G. L. Huang, and W. Lin, "Scanning angle extension of a millimeter wave antenna array using electromagnetic band gap ground," *IEEE Trans. Antennas Propag.*, vol. 70, no. 8, pp. 7264-7269, Aug. 2022.
- [9] X. Yang, Y. Liu, Y. X. Xu, and S. X. Gong, "Isolation enhancement in patch antenna array with fractal UC-EBG structure and cross slot," *IEEE Antennas Wireless Propag. Lett.*, vol. 16, pp. 2175-2178, May 2017.
- [10] M. Li, X. Chen, A. Zhang, W. Fan, and A. A. Kishk, "Split-ring resonator-loaded baffles for decoupling of dual-polarized base station array," *IEEE Antennas Wireless Propag. Lett.*, vol. 19, no. 10, pp. 1828-1832, Oct. 2020.
- [11] F. Faraz, X. Chen, Q. Li, J. Tang, J. Li, T. A. Khan, and X. Zhang, "Mutual coupling reduction of dual polarized low profile MIMO antenna using decoupling resonators," *Applied Computational Electromagnetics Society (ACES) Journal*, vol. 35, no. 1, pp. 38-43, Jan. 2020.
- [12] K. Wei, J. Li, L. Wang, Z. Xing, and R. Xu, "Mutual coupling reduction by novel fractal defected ground structure bandgap filter," *IEEE Trans. Antennas Propag.*, vol. 64, no. 10, pp. 4328-4335, Oct. 2016.
- [13] B. Qian, X. Chen, and A. A. Kishk, "Decoupling of microstrip antennas with defected ground structure using the common/differential mode theory," *IEEE Antennas Wireless Propag. Lett.*, vol. 20, no. 5, pp. 828-832, May 2021.
- [14] K. Wu, C. Wei, X. Mei, and Z. Zhang, "Array-antenna decoupling surface," *IEEE Trans. Antennas Propag.*, vol. 65, no. 12, pp. 6728-6738, Dec. 2017.
- [15] S. Zhang, X. Chen, and G. F. Pedersen, "Mutual coupling suppression with decoupling ground for massive MIMO antenna arrays," *IEEE Trans. Veh. Technol.*, vol. 68, no. 8, pp. 7273-7282, Aug. 2019.
- [16] S. Song, X. Chen, Y. Da, and A. Kishk, "Broadband dielectric resonator antenna array with enhancement of isolation and front-to-back ratio for MIMO application," *IEEE Antennas Wireless Propag. Lett.*, vol. 21, no. 7, pp. 1487-1491, Jul. 2022.
- [17] S. Song, Y. Da, B. Qian, S. Song, Y. Da, B. Qian, X. Huang, X. Chen, Y. Li, and A. A. Kishk, "Dielectric resonator magnetoelectric dipole arrays with low cross polarization, backward radiation, and mutual coupling for MIMO base station applications," *China Communications*, in press.
- [18] Y. Da, Z. Zhang, X. Chen, and A. A. Kishk, "Mutual coupling reduction with dielectric superstrate for base station arrays," *IEEE Antennas Wireless Propag. Lett.*, vol. 20, no. 5, pp. 843-847, May 2021.

- [19] Y. Da, X. Chen, and A. A. Kishk, "In-band mutual coupling suppression in dual-band shared-aperture base station arrays using dielectric block loading," *IEEE Trans. Antenna Propag.*, in press.
- [20] Y. M. Zhang and S. Zhang, "A novel aperture-loaded decoupling concept for patch antenna arrays," *IEEE Trans. Microw. Theory Techn.*, vol. 69, no. 9, pp. 4272-4283, Sept. 2021.
- [21] T. Dong, Y. Yu, M. Li, and H. Zeng, "Compact Antenna Array with Newly Designed Decoupling Network," *Applied Computational Electromagnetics Society (ACES) Journal*, vol. 33, no. 11, pp. 1196-1200, Nov. 2018.
- [22] B. Liu, Y. Da, X. Chen, and A. A. Kishk, "Hybrid decoupling structure based on neutralization and partition schemes for compact large-scale base station arrays," *IEEE Antennas Wireless Propag. Lett.*, vol. 21, no. 2, pp. 267-271, Feb. 2022.
- [23] Z. Ren, A. Zhao, and S. Wu, "MIMO antenna with compact decoupled antenna pairs for 5G mobile terminals," *IEEE Antennas Wireless Propag. Lett.*, vol. 18, no. 7, pp. 1367-1371, Jul. 2019.
- [24] L. Sun, H. Feng, Y. Li, and Z. Zhang, "Tightly arranged orthogonal mode antenna for 5G MIMO mobile terminal," *Microw. Opt. Technol. Lett.*, vol. 60, no. 7, pp. 1751-1756, Jul. 2018.
- [25] L. Sun, H. Feng, Y. Li, and Z. Zhang, "Compact 5G MIMO mobile phone antennas with tightly arranged orthogonal-mode pairs," *IEEE Trans. Antenna Propag.*, vol. 66, no. 11, pp. 6364-6369, Nov. 2018.
- [26] A. Zhang, K. Wei, Y. Hu, and Q. Guan, "High-isolated coupling-grounded patch antenna pair with shared radiator for the application of 5G mobile terminals," *IEEE Trans. Antennas Propag.*, in press.
- [27] F. Wei, X. B. Zhao, and X. W. Shi, "A balanced filtering quasi-Yagi antenna with low cross-polarization levels and high common-mode suppression," *IEEE Access*, vol. 7, pp. 100113-100119, Jul. 2019.
- [28] F. Wei, Z. J. Yang, P. Y. Qin, Y. J. Guo, B. Li, and X. W. Shi, "A balanced-to-balanced in-phase filtering power divider with high selectivity and isolation," *IEEE Trans. Microw. Theory Techn.*, vol. 67, no. 2, pp. 683-694, Feb. 2019.
- [29] L. Sun, Y. Li, Z. Zhang, and H. Wang, "Antenna decoupling by common and differential modes cancellation," *IEEE Trans. Antennas Propag.*, vol. 69, no. 2, pp. 672-682, Feb. 2021.
- [30] L. Sun, Y. Li, and Z. Zhang, "Decoupling between extremely closely spaced patch antennas by mode cancellation method," *IEEE Trans. Antennas Propag.*, vol. 69, no. 6, pp. 3074-3083, Jun. 2021.
- [31] X. Chen, P.-S. Kildal, J. Carlsson, and J. Yang, "MRC diversity and MIMO capacity evaluations of multi-port antennas using reverberation chamber and anechoic chamber," *IEEE Trans. Antennas Propag.*, vol. 61, no. 2, pp. 917-926, Feb. 2013.



**Yiran Da** received her B.S. degree in information engineering from Xi'an Jiaotong University, Xi'an, China, in 2020, where she is currently pursuing an M.S. degree. Her research interests include base station antenna design and mutual coupling reduction.



**Xiaoming Chen** (M'16-SM'19) received his B.Sc. degree in Electrical Engineering from Northwestern Polytechnical University, Xi'an, China, in 2006, and M.Sc. and PhD degrees in electrical engineering from Chalmers University of Technology, Gothenburg, Sweden, in 2007 and 2012, respectively. From 2013 to 2014, he was a postdoctoral researcher at the same university. From 2014 to 2017, he was with Qamcom Research & Technology AB, Gothenburg, Sweden. Since 2017, he has been a professor at Xi'an Jiaotong University, Xi'an, China. His research areas include MIMO antennas, over-the-air testing, reverberation chambers, and hardware impairments and mitigation. Prof. Chen serves as a Senior Associate Editor (AE) for *IEEE Antennas and Wireless Propagation Letters* and received the Outstanding AE Awards in 2018, 2019, 2020, and 2021. He received the URSI (International Union of Radio Science) Young Scientist Award in 2017 and 2018.



**Aofang Zhang** received his B.S. degree in Electromagnetic Wave Propagation and Antenna, and his Ph.D. degree in Electromagnetic Field and Microwave Technology from Xidian University, Xi'an, China, in 2014 and 2019, respectively. From 2019 to 2020, he was with the Consumer Business Group, Huawei Technologies Company Ltd., Xi'an. In 2021, he joined Honor Device Company Ltd., Xi'an, where he is currently a Senior Expert for the antenna design of smartphones, tablets, laptops, and routers. His current interests include antenna decoupling, multiband antennas, small size antennas, and MIMO antennas.



**Kunpeng Wei** received his B.S. degree in Electronic and Information Engineering from the Huazhong University of Science and Technology, Wuhan, China, in 2008, and his Ph.D. degree in electrical engineering from Tsinghua University, Beijing, China, in 2013. From July 2013 to December 2015, he was employed at the Radar Research Institute of the Chinese Air Force Research Laboratory, Beijing, conducting research in the areas of phased-array antenna design and radar system design. He joined the Consumer Business Group, Huawei Inc., Beijing, in 2016, where he was an Antenna Specialist and the Director of the Xi'an Antenna Team for five years. Since 2021, he has been with Honor Device Company Ltd., Beijing when this company split from Huawei; he is currently the Director of the Honor Antenna Team. He is also the leader of a large group of antenna engineers and is responsible for the research and development of antenna technologies to guarantee the market success of all Honor's mobile terminal products including smartphones, laptops, tablets, smartwatches, routers, smart screens, and earphones. He has authored over 50 refereed articles on consumer electronics antenna design. He holds over 15 granted U.S./Europe (EU)/Japan (JP)/China (CN) patents and has more than 30 patent applications pending. His current research interests include smartphone antenna design, small size 5G antenna systems in terminal devices, and millimeter-wave antenna array. Dr. Wei was a recipient of the Principal Scholarship of Tsinghua University in 2012, the Huawei Individual Gold Medal Award in 2018, the Huawei Team Gold Medal Award in 2017, and the Honor Team Gold Medal Award in 2021. He has been serving as an Associate Editor for *IET Electronics Letters* since October 2021.



**Ahmed A. Kishk** obtained his Ph.D. degrees in 1986 from the University of Manitoba, Canada. In 1986, he joined the University of Mississippi, first as an Assistant Professor and then as a Professor. Since 2011, he has been a Professor at Concordia University, Canada, as Tier 1 Canada Research Chair in Advanced Antenna Systems. He is a distinguished lecturer for the Antennas and Propagation Society (2013-2015). He was an Editor of *Antennas & Propagation Magazine* (1993-2014). He was an Editor-in-Chief of the *ACES Journal* from 1998 to 2001. He was a Guest Editor of the special issue on artificial magnetic conductors, soft/hard surfaces, and other complex surfaces, in *IEEE Transactions on Antennas and*

*Propagation*, 2005. He was the 2017 AP-S president. His research interests include millimeter wave antennas, beamforming network, dielectric resonator antennas, microstrip antennas, EBG, etc. He has published over 340-refereed journal articles and 450 conference papers. He is a co-author of four books, several book chapters, and the editor of three books. Prof. Kishk won the 1995 and 2006 outstanding paper awards for the *Applied Computational Electromagnetic Society Journal*. He received the 1997 Outstanding Engineering Educator Award from the Memphis section of the IEEE. He won the Outstanding Engineering Faculty Member of the Year in 1998 and 2009, and the Faculty Award for outstanding performance in research in 2001 and 2005. He received the Award of Distinguished Technical Communication for the entry of *IEEE Antennas and Propagation Magazine*, 2001. He also received The Valued Contribution Award for outstanding Invited Presentation from the Applied Computational Electromagnetic Society. He received the Microwave Theory and Techniques Society, Microwave Prize 2004 and 2013 Chen-To Tai Distinguished Educator Award from the IEEE Antennas and Propagation Society. He has been a Fellow of IEEE since 1998, Fellow of the Electromagnetic Academy, and a Fellow of the Applied Computational Electromagnetics Society (ACES).